

Three dimensional cross-sectional properties from bone densitometry

Tammy M. Cleek^{1,*}, Robert T. Whalen¹

5

¹Musculoskeletal Biomechanics Laboratory, NASA Ames Research Center, Moffett Field, California, USA

***Corresponding author. Current address:**

NASA Ames Research Center

10 MS 239-11

Moffett Field, CA 94035 USA

Tel (650) 604-0518

Fax (650) 604-3954

Email: tcleek@mail.arc.nasa.gov

15

Keywords: X-ray absorptiometry; Bone geometry; Moment of inertia; Tibia

Abstract

Bone densitometry has previously been used to obtain cross-sectional properties of bone in a single scan plane. Using three non-coplanar scans, we have extended the method to obtain the principal area moments of inertia and orientations of the principal axes at each cross-section along the length of the scan. Various aluminum phantoms were used to examine scanner characteristics to develop the highest accuracy possible for *in vitro* non-invasive analysis of mass distribution. Factors considered included x-ray photon energy, initial scan orientation, the included angle of the 3 scans, and I_{min}/I_{max} ratios. Principal moments of inertia were accurate to within 3.1% and principal angles were within 1° of the expected value for phantoms scanned with included angles of 60° and 90° at the higher x-ray photon energy. Low standard deviations in error also indicate high precision of calculated measurements with these included angles. Accuracy and precision decreased slightly when the included angle was reduced to 30°. The method was then successfully applied to a pair of excised cadaveric tibiae. The accuracy and insensitivity of the algorithms to cross-sectional shape and changing isotropy (I_{min}/I_{max}) values when various included angles are used make this technique viable for future *in vivo* studies.

1. Introduction

The most widely used and accepted method of non-invasive skeletal assessment is x-ray absorptiometry which measures bone mineral content and areal bone mineral density. Although these measures have been useful in detecting regional changes in bone mass, whole bone stiffness and strength are not just dependent on the amount of material present, but also upon cross-sectional shape and distribution of the bone mass.

In keeping with this idea, densitometric methods have been applied to obtain cross-sectional properties (area, moment of inertia) of bone in a single scan plane (Martin and Burr, 1984). This single plane method has been applied to the femoral neck and femoral, tibial, and fibular shafts with results indicating geometric properties may be better predictors of bone strength than mass measurements alone, as well as being risk factors for stress fracture (Beck et al., 1990, 1996, 2000; Milgrom et al., 1989). Multiple scans analyses have also been used to compute principal moments in sections of the distal radius that were predictive of fracture load and were also highly correlated to calculations from digitized sections (Myers et al., 1991, 1993).

Principal moments and orientations may be computed from a minimum of 3 non-coplanar scans using standard formulations for reference axes rotations (Timoshenko, 1976). We investigated the precision and accuracy of this method with respect to x-ray energy, orientation to the scan plane, the total included angle spanned by the three scans, and flexural symmetry by using a variety of aluminum phantoms and then applying the method to cadaveric tibiae. The results of these investigations will determine the feasibility of the method for future *in vivo* use, particularly in the lower leg.

2. Methods

2.1 Theory

Any cross-section of arbitrary shape has, in general, a maximum and a minimum area moment of inertia about orthogonal axes that pass through the area centroid. These principal moments and their orientations can be obtained from any three area moments of inertia of the cross-section computed about known axes. The accuracy of the computed principal moments and their orientation will also depend, in general, on the angular separation between the three axes. We used the method of Martin and Burr (1984) to obtain, from x-ray attenuation profiles, cross-sectional area moments of inertia about each of three axes separated by known angular rotations. We then used the three area moments and known separation angles to calculate the principal moments and their orientation with respect to a particular reference frame using standard equations (Figure 1). Details of computations are included in Appendix I.

2.2 Phantom designs

Our method was tested with aluminum phantoms including: a circular tube, an eccentric circular tube, and a more complex tubular phantom with tapering helical slots (Figure 2). All phantoms were machined from the same ingot and dimensions were selected to provide a magnitude and range of principal moments within the values expected for human tibiae. The circular tube, because of its symmetry, was used to investigate the effect of x-ray photon energy on computed properties in the single plane. Minimizing errors in the single plane measurement was important since three such values would be carried into the calculation of principal moments. The eccentric circular tube was used to look at the effect of initial orientation of the phantom and the angular

separation between scans on the computations. The helical phantom was used primarily to investigate the effect of isotropy, defined as I_{min}/I_{max} (range: 0.486 to 1.0), a measure of flexural symmetry. In addition, the sharp edges (high thickness gradients) and rapidly changing areal properties and principal axes orientation along the length of the helical phantom provided a robust test of the method. Principal moments and orientations were computed every millimeter along the length, increasing the dependence of accuracy on image noise and multi-scan registration accuracy. Expected values of all sectional properties were computed from micrometer measurements or were set by the machining operation.

The right and left embalmed tibiae of an elderly female were used for further validation. The proximal end of each excised tibia was potted in a fixture with the medio-lateral direction parallel to a reference surface machined on the fixture.

2.3 Scanning procedure

All scans were taken with a Hologic QDR-1000/W (Waltham, MA) bone densitometer using the spine scan mode (point spacing: 0.951mm, line width: 1.003mm). All phantoms were scanned in air; tibiae were scanned in a 10 cm water bath to allow for "soft tissue" attenuation subtraction.

The phantoms and tibiae were held in a precision indexer (0.1° resolution) during scanning. The rotational axis of the indexer was aligned parallel to the length of the scan table. The circular tube was scanned once due to its symmetry. Remaining phantoms and tibiae were scanned along their entire length in multiple orientations. Following scanning in one plane, the scanner arm returned to a "home" position, the object was rotated to a new position with the indexer, and another scan taken, ensuring scan lines containing cross-sectional data would not be offset by more than a fraction of a line width. The eccentric circular tube was scanned from -90° to $+90^\circ$ in 15° increments from the reference orientation (13 scans). The helical phantom was scanned in 15° increments from -45° to $+45^\circ$ of the reference orientation (7 scans). The tibiae were scanned at $+45^\circ$, 0° , and -45° of the reference surface.

2.4 Calibration and scan processing

An aluminum calibration phantom consisting of twenty 1.27 mm high steps was used to calibrate attenuations to equivalent aluminum thicknesses. Similarly, a set of dense cortical bovine step wedges (20 steps, range: 1.3-27.4 mm, wet density: $2.10 \pm 0.05 \text{ g/cm}^3$) scanned in a 10 cm water bath was used to calibrate tibial scan attenuations to bone tissue thicknesses. The QDR-1000/W has a three-compartment internal calibration wheel that rotates continuously during scanning with air, bone-equivalent, and tissue-equivalent segments. X-rays from alternating high- and low-energy spectra (70, 140 kVp) pass through the object and one wheel segment per pixel in a repetitive sequence. Consequently, three high- and three low-energy calibration equations corresponding to the wheel segments were determined by non-linear regression analysis of x-ray attenuation values and corresponding step thicknesses for each calibration phantom.

To achieve maximum accuracy, we extracted high- and low-energy pixel attenuation values from the raw data files and analyzed them separately. The attenuations were transformed by subtracting a line by line average offset from each pixel computed from points known to have passed only through air or the water bath above the table. Pixel attenuations from aluminum phantoms and tibiae were converted to equivalent thicknesses of aluminum and bone tissue respectively. The region immediately surrounding the specimen was identified and the attenuation values for all pixels falling outside this region were set to zero. No edge-corrections were made.

Cross-sectional area, centroid, and moment of inertia in the plane of the scan were computed from the thickness values and principal moments and principal axis orientations were computed from three scan analyses as previously described.

Cross-sectional properties of the helical phantom were computed from three scans each sweeping included angles of 30° ($+15^\circ, 0^\circ, -15^\circ$), 60° ($+30^\circ, 0^\circ, -30^\circ$), and 90° ($+45^\circ, 0^\circ, -45^\circ$) centered about a reference axis. The eccentric circular tube phantom was analyzed in the same manner but at seven initial orientations formed by sweeping the reference plane in 15° increments from 0° to 90° . Cross-sectional properties of each of the tibiae were computed from the three scans with an included angle of 90° .

3. Results

Errors in calculated section properties for the phantoms are reported in Table 1. Computed properties for the circular tube were averaged over 10 lines. Computed thickness profiles indicate that most errors occur at the edges of the internal diameter where the thickness gradient is the largest. High photon energy calibrations were more accurate in predicting aluminum thicknesses resulting in area and moment of inertia being underestimated by only 1-2%. The low standard deviation indicates little line to line variability and high precision of the measurements. The precision values were on the order of reported machine precision for bone mass measurements.

Eccentric tube properties were not significantly dependent on the initial orientation of the phantom principal axis and were therefore averaged together, yielding an expected accuracy and a conservative estimate of precision. Computed principal moments and orientation of principal axes were very accurate for all included angles with principal moments underestimated by less than 3.4% and principal angles were within half a degree of expected values for all scan combinations using high energy calibrations. Although accuracy was quite independent of the included angle, precision was not as robust, as indicated by a slightly increased standard deviation at 30°.

Errors in computed principal moments and orientation of the principal major axis along the length of the tapered-slot helical phantom for isotropy range from 0.49 to 0.80 were also comparable for all included angles. Errors in principal axis orientation increased slightly with decreasing included angle, but were less than 1° for included angles of 90° and 60°. The error increased slightly to 3° when the included angle was further reduced to 30°. At higher isotropy values (>0.8), errors in orientation increased as expected, since the helix approaches a cylinder with no unique principal axes.

Profiles of the principal moments, principal axis orientations, and isotropy index for the right and left tibia matched up remarkably well (Figure 3). The principal moments in the tibiae were larger in the proximal ends and the values approached each other along the shaft towards the distal end. The isotropy index for the tibiae ranged from 0.4 to 0.8 between 20% and 80% of its length. The principal major axis of the tibiae is oriented between the medial and posterior directions.

4. Discussion

Our initial efforts have concentrated on optimizing our technique for accuracy and validating our algorithms using phantoms of known material properties and geometries. Excellent agreement was found between experimentally determined and true sectional properties of axi- and non-axi-symmetric aluminum phantoms.

5 Analyses with the high energy proved to be more accurate than low, highlighting the common problem of non-linear calibration at edges. These edge problems may be corrected with a high pass deconvolution filter with beam characteristics, which we intend to include in future studies. The low energy, although slightly less accurate, may still be preferable in certain cases since it provides a larger dynamic range. However, with our two-component systems (aluminum and air, bone and "soft tissue"), a single high energy analysis is more
10 accurate than a combination of both energies since beam hardening effects are corrected by direct calibrations.

The results of the eccentric circular tube and tapered helix show computed properties are relatively insensitive to phantom orientation and included angles of 30°, 60° and 90°. This finding is important for future *in vivo* studies of bones such as the tibia, which must be scanned without interference from the fibula, thus requiring more acute angles.

15 In applying the method to excised tibiae, results were promising and showed remarkable bilateral symmetry in geometric properties. Our *ex vivo* analyses using single energy analyses with a constant thickness water bath for a two-component system effectively eliminates non-bone-tissue artifacts. However, future application of the method *in vivo* are complicated by the fact that in addition to bone, there is overlying fat and lean mass, intramedullary bone marrow, and fluid filling the bone porous regions, each with different
20 attenuation properties. Dual-energy calculations could be incorporated to eliminate the need for a constant thickness soft tissue equivalent, although this would inherently decrease accuracy.

In conclusion, our technique provides a quick, accurate, and non-invasive way to obtain three-dimensional structural quantities that contribute to the flexural, axial, and (approximately) torsional rigidity, and therefore, stiffness of long bones.

Acknowledgments

This study was supported by NASA Grant 199-26-12-34. The authors thank B. Jenny Kiratli, PhD for the generous use of her DXA machine.

5 References

- Beck, T.J., Ruff, C.B., Warden, K.E., Scott, W.W., Rao, G.U., 1990. Predicting femoral neck strength from bone mineral data: A structural approach. *Investigative Radiology* 25, 6-18.
- Beck, T.J., Ruff, C.B., Mourtada, F.A., Shaffer, R.A., Maxwell-Williams, K., Kao, G.L., Sartoris, D.J., Brodine, S., 1996. Dual-energy X-ray absorptiometry derived structural geometry for stress fracture prediction^k in male U.S. Marine Corps recruits. *Journal of Bone and Mineral Research* 11, 645-53.
- 10 Beck, T.J., Ruff, C.B., Shaffer, R.A., Betsinger, K., Trone, D.W., Brodine, S.K., 2000. Stress fracture in military recruits: gender differences in muscle and bone susceptibility factors. *Bone* 27, 437-444.
- Martin, R.B. and Burr, D.B., 1984. Non-invasive measurement of long bone cross-sectional moment of inertia by photon absorptiometry. *Journal of Biomechanics* 17, 195-201.
- 15 Milgrom, C., Giladi, M., Simkin, A., Rand, N., Kedem, R., Kashtan, H., Stein, M., Gomori, M., 1989. The area moment of inertia of the tibia: a risk factor for stress fractures. *Journal of Biomechanics* 22, 1243-8.
- Myers, E.R., Sebeny, E.A., Hecker, A.T., Corcoran, T.A., Hipp, J.A., Greenspan, S.L., Hayes, W.C., 1991. Correlations between photon absorption properties and failure load of the distal radius in vitro. *Calcified Tissue International* 49, 292-7.
- 20 Myers, E.R., Hecker, A.T., Rooks, D.S., Hipp, J.A., Hayes, W.C., 1993. Geometric variables from DXA of the radius predict forearm fracture load in vitro. *Calcified Tissue International* 52, 199-204.
- Timoshenko, S., 1976. *Strength of Materials*. D. Van Nostrand Company, Inc, New Jersey, pp. 351-355.

APPENDIX A

From Martin and Burr (1984) cross-sectional area, A , the centroid of the area, x^* , and the cross-sectional area moment of inertia, I_y about an axis passing through the centroid, were calculated using discrete forms of equations (1-3). In the equations x_i is the distance from an arbitrary origin to the midpoint of the pixel, Δx is the pixel width of the scan mode and t_i is the material thickness at the i th pixel.

$$A = \int dA \sim \sum t_i \Delta x \quad (1)$$

$$x^* = (1/A) \int x dA \sim (1/A) \sum x_i t_i \Delta x \quad (2)$$

$$I_y = \int (x^2 - x x^*) dA \sim \sum (x_i^2 - x_i x^*) t_i \Delta x \quad (3)$$

Values of I_y , I_{y+} , and I_{y-} for three non-coplanar scans at known rotations ($\pm\Theta$ about the y -axis, see Figure 1b) computed from equations (1-3) are used to compute I_x and the cross-product term, I_{xy} , from which the principal moments of inertia and principal angle are obtained from the following equations.

$$I_{xy} = (I_{y+} - I_{y-}) / (4 \cos\Theta \sin\Theta) \quad (4)$$

$$I_x = (I_{y+} + I_{y-} - 2 I_y \cos^2\Theta) / (2 \sin^2\Theta) \quad (5)$$

$$I_{\min} = (I_x + I_y)^{1/2} - ((I_x + I_y)/4 + (I_{xy})^2)^{1/2} \quad (6)$$

$$I_{\max} = (I_x + I_y)^{1/2} + ((I_x + I_y)/4 + (I_{xy})^2)^{1/2} \quad (7)$$

$$\Theta_p = 1/2 (\arctan (2 I_{xy} / (I_y - I_x))) \quad (8)$$

Since the angle, given by equation (8), is only defined uniquely for values between $\pm 45^\circ$, the angle computed from equation (8) may identify the orientation of either the major or the minor principal axis, depending upon which principal axis lies within the domain $\pm 45^\circ$. The sign of the product of inertia term, I_{xy} , and the magnitude of I_x relative to I_y can be used to identify whether Θ_p is the orientation of the major or minor principal axis. Once this has been done, Θ_p can be adjusted, if necessary, to indicate the orientation of the principal major axis.

Conditions (9a-9h) examine the product of inertia term and magnitude of the moments of inertia in order to assign the orientation of the principal major axis to the first and fourth quadrants of a right-handed

x-y coordinate system. Cases 9d through 9h are special test conditions that account for: axi-symmetric cross-sections (9d); the principal major axis oriented exactly $\pm 45^\circ$ with respect to the reference axis (9e,f); and the principal major axis aligned parallel to *or* perpendicular to the reference axis (9g,h).

$$\text{if } I_{xy} > 0 \text{ \& } I_y > I_x, \Theta_p = \Theta_p \quad (9a)$$

$$5 \quad \text{if } I_{xy} < 0 \text{ \& } I_y < I_x, \Theta_p = \Theta_p - 90 \quad (9b)$$

$$\text{if } I_{xy} > 0 \text{ \& } I_y < I_x, \Theta_p = \Theta_p + 90 \quad (9c)$$

$$\text{if } I_{xy} = 0 \text{ \& } I_x = I_y, \Theta_p = 0; \quad (9d)$$

$$\text{if } I_{xy} < 0 \text{ \& } I_x = I_y, \Theta_p = -45; \quad (9e)$$

$$\text{if } I_{xy} > 0 \text{ \& } I_x = I_y, \Theta_p = 45; \quad (9f)$$

$$10 \quad \text{if } I_{xy} = 0 \text{ \& } I_y > I_x, \Theta_p = 0; \quad (9g)$$

$$\text{if } I_{xy} = 0 \text{ \& } I_y < I_x, \Theta_p = 90; \quad (9h).$$

Captions:

- Figure 1. a) The cross-sectional area (shaded region), centroid, and area moment of inertia in the scan plane are computed by integrating the thickness, t , across the scan width. b) Principal moments of inertia and orientation of the principal axes (clockwise positive) are determined from the analyses of 3 registered non-coplanar scans. The coordinate system for the principal axis orientation for the right tibia as viewed from the distal end is shown. The coordinate system for the left tibia is a "mirror image" to facilitate comparisons of bilateral symmetry.
- Figure 2. Aluminum phantom designs with idealized cross-sections for 1) circular tube, OD: 3.11cm, ID: 1.93 cm, 2) eccentric circular tube, OD: 3.17cm, ID: 2.22cm, center offset by 0.35 cm, and 3) helical tapered phantom, OD: 3.18cm, ID: 1.91cm, slot width: 0.79cm, helical slots offset by 180°, depth linearly tapered from 0.65 cm to 0 over 1.5 revolutions.
- Table 1. Error in calculated section properties for various aluminum phantoms. Circular tube data at high and low photon energy levels are computed from an average of 10 scan lines. Eccentric circular tube data are computed from 7 different initial orientations using an average of 10 scan lines. Helical taper tube data are average errors along the length of the phantom for I_{min}/I_{max} ranging from 0.49-0.80.
- Figure 3 a) Computed principal moments along the length of the tibiae. Isotropy values (I_{min}/I_{max}) range from 0.4-0.8. b) Computed principal angles along the length of the tibiae. Coordinate frame (viewed distally): 0° medial, +90° anterior, -90° posterior (see Figure 1b). The right and left tibiae, in effect, "mirror" each other.

Figure 1

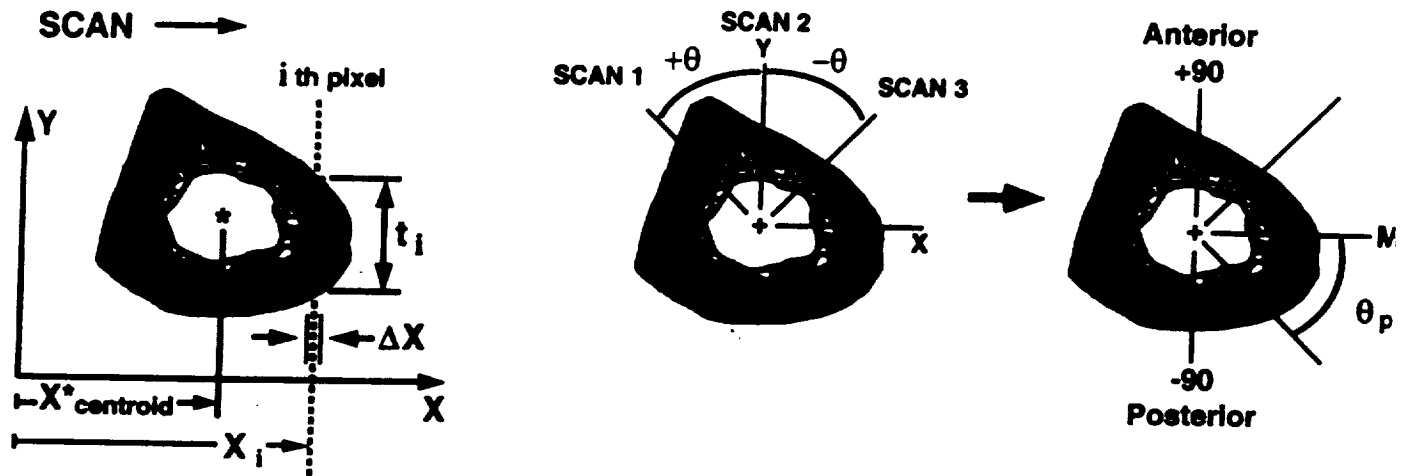


Figure 2

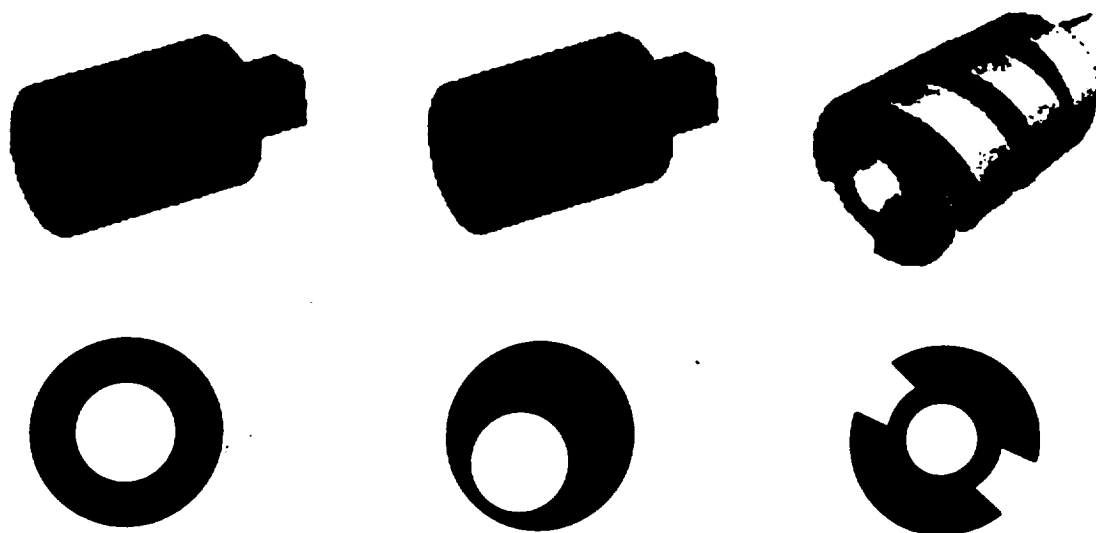


Table 1

Phantom design	Property	Energy	Scan configuration		
Circular tube	Area (%)	hi	Single scan plane		
	lo				
	I (%)	hi			
		lo			
			Included angle for 3 scans		
			90°	60°	30°
Eccentric circular tube	I _{max} (%)	hi	-2.74 ± 1.03	-2.72 ± 1.27	-2.74 ± 2.19
	I _{min} (%)	hi	-3.04 ± 0.68	-3.09 ± 0.96	-3.36 ± 2.53
	Principal Angle (deg)	hi	-0.31 ± 1.10	-0.30 ± 1.38	-0.36 ± 2.80
Helical taper tube	I _{max} (%)	hi	2.40 ± 1.09	2.90 ± 1.84	2.55 ± 4.50
	I _{min} (%)	hi	1.38 ± 1.49	1.34 ± 1.67	2.02 ± 5.28
	Principal Angle (deg)	hi	0.01 ± 1.12	1.00 ± 1.72	2.61 ± 3.55

Figure 3

